Quasiparticle alignments and α-decay fine structure of ^{175}Pt

P. Peura,[1,*] C. Scholey,[1] D. T. Joss,[2] S. Juutinen,[1] R. Julin,[1] T. Bäck,[3] B. Cederwall,[3] P. T. Greenlees,[1] U. Jakobsson,[1] P. Jones,[1,†] D. S. Judson,[2,‡] S. Ketelhut,[1,§] M. Labiche,[4] M. Leino,[1] M. Nyman,[1] D. O'Donnell,[4] R. D. Page,[2] P. Rahkila,[1] P. Ruotsalainen,[1] M. Sandzelius,[1] P. J. Sapple,[2] J. Sarén,[1] J. Simpson,[4] J. Thomson,[2] J. Uusitalo,[1] and H. V. Watkins[2,‖]

[1]*Department of Physics, University of Jyväskylä, P.O. Box 35, FI-40014 Jyväskylä, Finland*
[2]*Oliver Lodge Laboratory, University of Liverpool, Liverpool L69 7ZE, United Kingdom*
[3]*Department of Physics, Royal Institute of Technology, Stockholm SE-10691, Sweden*
[4]*STFC Daresbury Laboratory, Daresbury, Warrington WA4 4AD, United Kingdom*
(Received 10 January 2014; published 24 February 2014)

Excited states and decay properties of ^{175}Pt have been investigated using the ^{92}Mo(^{86}Sr,$2pn$) fusion-evaporation reaction. The JUROGAM I γ-ray spectrometer and the GREAT spectrometer were used in conjunction with the gas-filled recoil separator RITU for the measurement of the radiation at the target and focal plane positions, respectively. Two new band structures, assigned to be based on the $I^\pi = (7/2^-)$ ground state in ^{175}Pt, have been established and the known yrast band has been extended up to $I^\pi = (49/2^+)$. Rotational properties of the excited states in ^{175}Pt have been investigated within the cranked shell-model formalism. The low-frequency changes in the alignments of the positive- and negative-parity bands are interpreted as a sign of proton-pair excitations in the rotating core. Furthermore, the α-decay measurements reveal a candidate for a fourth α-decay branch in ^{175}Pt, feeding a non-yrast state in ^{171}Os.

I. INTRODUCTION

Low-spin states of neutron-deficient platinum nuclei $^{174-176}$Pt are known to display characteristics that are interpreted as signs of shape coexistence [1–4]. The ground states of these nuclei are predicted to have triaxially deformed shapes according to potential energy surface (PES) and total Routhian surface (TRS) calculations. For the higher-lying coexisting configuration a prolate deformation is predicted, whereas in the heavier platinum isotopes, $A = 180–186$, this configuration is observed to become the ground state [2,5–7]. The well deformed and the weakly deformed configurations are predicted to be almost degenerate in ^{178}Pt [8], and in the lighter platinum $A \leqslant 176$ isotopes the weakly deformed configuration forms the ground state [3,9–11]. Thus, ^{175}Pt is situated in a transitional region, where the weakly deformed triaxial configuration forms the ground state, but a well deformed configuration is sufficiently low lying to cause perturbations in the measured yrast band.

The investigation of rotational bands of odd-mass nuclei yields information on the single-particle orbitals occupied by the last odd nucleon and the coupling of this nucleon to the core. In ^{175}Pt the neutron Fermi surface is situated close to the $f_{7/2}$, $h_{9/2}$, and $i_{13/2}$ spherical shell-model orbitals. Excited states in ^{175}Pt, based on the mixed $i_{13/2}$ band head, have been

reported earlier by Cederwall *et al.* [2], who interpreted the low-frequency anomalies of the positive-parity band as being caused by a crossing of two zero-quasiparticle configurations. At high spin an $(i_{13/2})^2$ quasineutron alignment was assumed to take place. In the neighboring odd-A nucleus ^{177}Pt, the ground-state configuration was assumed to be based on the $5/2^-$[512] Nilsson orbital, with the $1/2^-$[521] and the $i_{13/2}$ band heads lying only 148 and 95 keV above the ground state, respectively. No effects pointing towards shape coexistence in ^{177}Pt were observed [12].

In present work we report, for the first time, an observation of excited negative-parity states in ^{175}Pt. In addition, the known positive-parity band has been extended up to $I^\pi = (49/2^+)$. The cranked shell-model (CSM) formalism has been utilized in the interpretation of the high-spin structure of the excited states. Furthermore, the α-decay properties of ^{175}Pt have been investigated, leading to the observation of an α-decay branch from ^{175}Pt to a $I^\pi = (9/2^-)$ 207.9-keV state in ^{171}Os.

II. EXPERIMENTAL DETAILS

Excited states in ^{175}Pt were populated in the ^{92}Mo(^{86}Sr,$2pn$) fusion-evaporation reaction. The strontium beam was accelerated by the K130 cyclotron to an energy of 403 MeV at the Accelerator Laboratory of the Department of Physics, University of Jyväskylä (JYFL), Finland. The enrichment of the self-supporting 600-μg/cm^2 thick ^{92}Mo target was 98 %. A 40-μg/cm^2 thick carbon reset foil was positioned behind the target. The beam intensity during 7 days of beam time was on average 8 pnA.

Prompt γ rays emitted at the target position were detected by the JUROGAM I detector array. The array consisted of 43 EUROGAM Phase 1 [13] and GASP [14] type germanium detectors, each surrounded by an anti-Compton bismuth germanate (BGO) shield. The absolute photo-peak efficiency

of JUROGAM I was 4.2% at 1.3 MeV and the average energy resolution was 2.7 keV at 1.3 MeV. Recoiling fusion products (recoils) were separated from beam particles and fission products by the gas-filled separator RITU [15]. At the focal plane of RITU the recoils and their decay products were detected with the GREAT spectrometer [16]. Within GREAT the recoils first passed through a multiwire proportional counter (MWPC), where their energy loss and position were recorded. After the MWPC the recoils were implanted into two adjacent 300-μm thick double-sided silicon strip detectors (DSSD). Looking from upstream the 60 vertical strips and the 40 horizontal strips are located at the front and back sides of the DSSD, respectively. Downstream from the DSSD, behind a 500-μg/cm^2 thick beryllium window, was a segmented planar germanium detector for low-energy γ-ray detection. High-energy γ rays were detected with a segmented Clover germanium detector, which was located directly above the focal-plane chamber. Upstream from the DSSD an array of 28, 500-μm thick, silicon PIN detectors was located perpendicular to the front face of the DSSDs. They were used for conversion-electron and escape α-particle detection. The internal α-particle energy calibration was performed using the online α-decay data. The α-particle energies of $^{169,170-172}$Os and ^{174}Pt were used for the α-particle energy calibration [17]. The cross section for the $2pn$ evaporation channel was estimated to be 4 mbarn. An average ^{175}Pt α-particle rate of 135 s^{-1}, RITU transmission of 40% and full-energy α-particle detection efficiency of 50% were assumed in the calculation of the number of ^{175}Pt recoils produced during the experiment.

The data acquisition in the experiment was performed using the GREAT total data readout (TDR) method [18], where an individual detector channel receives an event time-stamp from a global 100 MHz clock. All the single-channel data streams from the JUROGAM I array and the GREAT spectrometer were merged together into one data stream before storage. The raw events were prefiltered online taking 5 μs of data before any focal-plane event. The data analysis was undertaken using the GRAIN [19] and RADWARE [20,21] software packages. The target position γ-ray data were analyzed using the recoil-gated (RG) JUROGAM I double- and triple-coincidence data. The results were further verified by using the recoil-decay tagging (RDT) technique [22,23]. The time condition for the double- and triple-coincidence γ ray events was 100 ns. The fine-structure α decay of ^{175}Pt was studied using asymmetric α-γ and α-conversion-electron matrices.

III. RESULTS

A. Decay spectroscopy

The half-life of the ^{175}Pt α decay was determined to be 2.53(6) s [24], based on results from previous studies. The main goal of the present experiment was the RDT study of ^{175}Hg, which has a half-life of 11 ms [25]. For this reason, the total event count-rate of the DSSD was on average 1 kHz during the experiment, which is not an optimal rate for unambiguous ^{175}Pt recoil-α correlations. However, because the event distribution was not even in the horizontal strips of the DSSD, the low count-rate peripheral strips of the DSSD
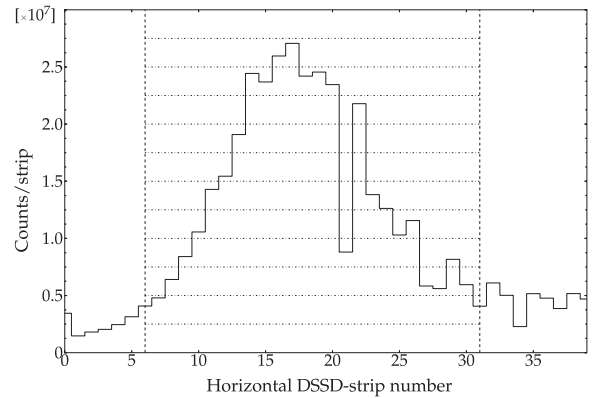

FIG. 1. The distribution of detected events across the horizontal strips of the DSSD during the whole experiment (solid line). The high count-rate area that is not used for looking for correlations is indicated (horizontal dot-dash lines). The remaining edge area was used for recoil-α time correlations in cases where indicated in the text.

were used for the RDT analysis of ^{175}Pt [26]. The event distribution and the selection made on the horizontal strips are shown in Fig. 1. With this method the average event rate is lowered by a factor of 6. Figure 2(a) shows the total α-particle energy spectrum obtained in the experiment, using only the
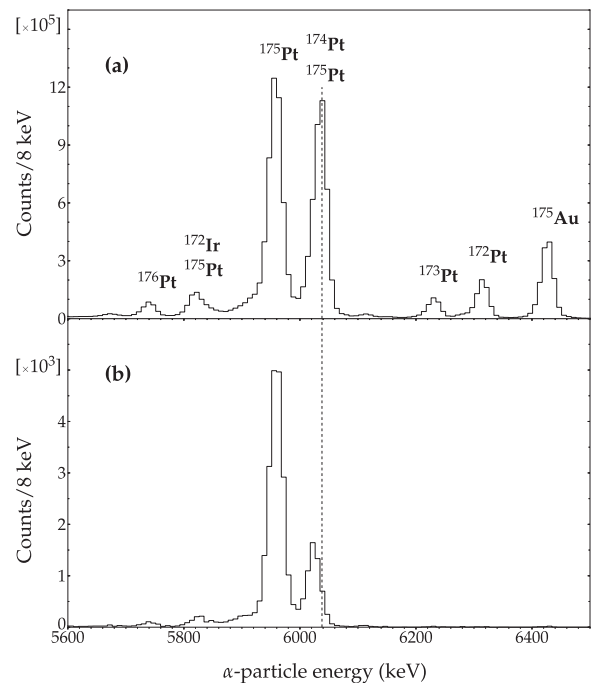
FIG. 2. Total α-particle energy spectrum with a 7.5 s coincidence window for recoil-α correlation (a). The α-particle energy spectrum, which is tagged with prompt JUROGAM γ rays (b). The prompt γ rays used for tagging were 328.6 keV, 423.2 keV, and 436.4 keV. The recoil-α time-coincidence window of (1.8–7.5) s was used for spectrum (b) in order to reduce the contribution of the faster α decay of ^{174}Pt. Only the low count-rate border area of the DSSD was used for the search of recoil-α correlations.

TABLE I. Decay spectroscopy data extracted from this experiment. For the ^{175}Pt ground state half-life a weighted average value of the fitted half-lives 2.43(4) s is used. The half-lives are fitted to the recoil-α time-difference spectra, using the low count-rate horizontal strips of the DSSD for the recoil-alpha correlations. The reduced widths and the hindrance factors are calculated using the Rasmussen method [41] and the weighted average value for the half-life. The $\delta^2_{\mathrm{Ref}} = \frac{1}{2}(\delta_1^2 + \delta_2^2) = 109$ keV is taken according to Ref. [42], where the values for the nearest even-even neighbors, ^{174,176}Pt, are used.

Nucleus	E_α (keV)	$t_{\frac{1}{2}}$ (s)	b_α (%)	$\delta^2 = \lambda_\alpha h P^{-1}$ (keV)	Hindrance factor	J_f^π	E_γ (keV)	α_k
^{174}Pt	c[a]	0.93(3)						
^{171}Ir	5919(4)	1.14(5)[b]					91.7(4)	
^{172}Ir	5817(4)	1.81(4)[c]					161.6(4)	
^{175}Pt	5814(4)	2.6(3)[d]	4.0(9)[h]	17(4),30(7)	6(2),3.6(8)	$(7/2^-),(9/2^-)$	211.2(5)	
		2.34(8)[e]					134.1(4)	2.1(2)[i]
							76.7(3)	11.6(9)
	5819(4)		0.7(2)[h]	5(2)	20(6)	$(9/2^-)$	207.9(5)	
							130.8(4)	2.1(2)[i]
							76.7(3)	11.6(9)
^{175}Pt	5948(4)	2.39(5)[f]	55(5)[j]	64(6)	1.7(2)	$(7/2^-)$	76.7(3)	
^{175}Pt	6021(4)	2.39(6)[g]	4.8(8)[j]	5.0(9)	22(4)	$(5/2^-)$		

[a]Used for calibration.
[b]$E_\gamma = 91.7$ keV in coincidence with $E_\alpha = 5919$ keV is demanded.
[c]$E_\gamma = 161.6$ keV in coincidence with $E_\alpha = 5817$ keV is demanded.
[d]$E_\gamma = 207.9$ keV, 211.2 keV in coincidence with $E_\alpha = 5814$ keV, 5819 keV are demanded.
[e]$E_\gamma = 130.8$ keV, 134.1 keV in coincidence with $E_\alpha = 5814$ keV, 5189 keV are demanded.
[f]$E_\gamma = 76.7$ keV in coincidence with $E_\alpha = 5948$ keV is demanded.
[g]The prompt $E_\gamma = 328.6$ keV in delayed coincidence with $E_\alpha = 6021$ keV is demanded.
[h]$b_\alpha = 4.7\%$ [29] is divided by the total intensity ratio of the 130.8-keV and 134.1-keV transitions.
[i]This is the calculated value for both the 130.8 keV and 134.1 keV transitions together.
[j]The value is from Ref. [29].

low-counting strips of the DSSD defined in Fig. 1. All the half-lives measured in this work were obtained from the data where only the low-counting horizontal DSSD strips are used for the search of recoil-α correlations. The α-decay properties of ^{175}Pt were studied, for the first time, by Siivola [27] and later by Gauvin *et al*. [28]. The fine structure of the α decay of ^{175}Pt was reported, for the first time by Hagberg *et al*. [29]. The α-particle energies were reported to be 5831(10), 5964(5), and 6038(10) keV, with absolute α-decay branching ratios of 4.7(10)%, 55(5)%, and 4.8(8)%, respectively. The γ-ray energies observed in coincidence with the α decays were reported to be 76.4(10), 134.4(10), and 211.8(10) keV [29].

Gamma rays promptly following the α decay of a mother nucleus to the excited states in the daughter nucleus provide a clean tag for the α-decay events. Indeed, the whole DSSD can be used for the α-particle energy measurement in these cases despite the high event rate for recoil-α event correlations. However, the excited state in the daughter nucleus can also decay via the emission of a conversion electron. In this case the measured energy will be the sum of the absorbed electron energy and the α-particle energy [30]. The α-particle energies for ^{175}Pt from this experiment are given in Table I and the deduced α-decay level scheme is shown in Fig. 3. The ^{174}Pt α-particle energy of 6038(4) keV, with $t_{\frac{1}{2}} = 0.89(2)$ s [31], overlaps with the ground-state to ground-state α-particle energy of ^{175}Pt. Since the $E_\alpha = 6021(4)$-keV decay branch in ^{175}Pt is only 4.8%, the ^{174}Pt α-decay events dominate the spectrum at this energy in Fig. 2(a). Tagging with the prompt

328.6-keV, 423.2-keV, and 436.4-keV ^{175}Pt in-beam γ rays provides a clean selection for the α decays of ^{175}Pt. The result of the prompt tagging of the α decays is shown in Fig. 2(b), where only the low-counting strips of the DSSD were used in the search of recoil-α correlations (see Fig. 1). Due to the uncertainties caused by conversion-electron summing, the α-decay branching ratios were taken from Ref. [29].

Figure 4(a) shows γ rays detected at the focal-plane planar detector within 150 ns of the detection of the $E_\alpha = 5814$-keV
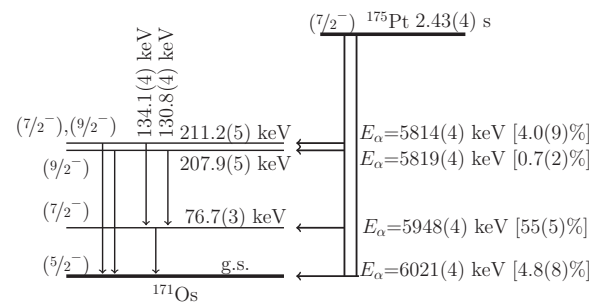
FIG. 3. The α-decay scheme of ^{175}Pt to the ground state of the daughter nucleus ^{171}Os. The absolute α-decay branching ratios for the 6021-keV and 5948-keV transitions are from the work by Hagberg *et al*. [29]. The α-branching ratio given by Hagberg *et al*. for the two lowest energy α decays has been divided into two parts, using the ratios of the total intensities of the 130.8-keV and the 134.1-keV transitions detected at the focal plane planar detector.
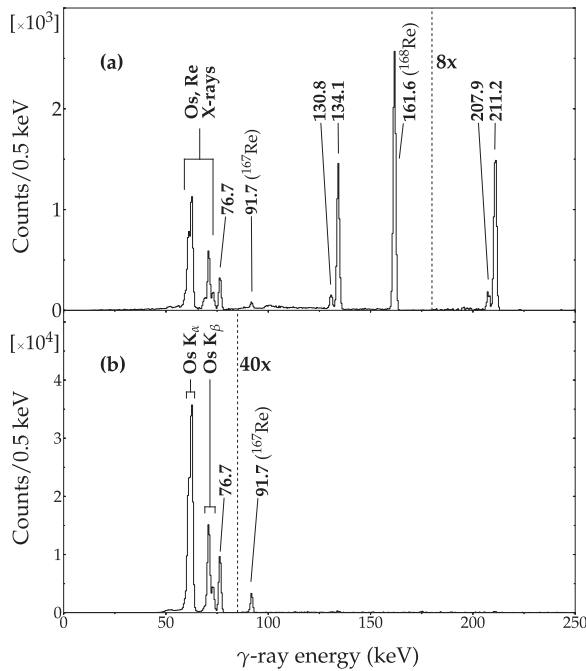
FIG. 4. Gamma rays in coincidence with the 5814-keV and 5819-keV ^{175}Pt α particles within 150 ns (a) and γ rays in coincidence with the 5948-keV ^{175}Pt α particles within 150 ns (b). The events in both figures were detected by the planar detector and the whole DSSD was used for the α particle detection. The coincidence of the 91.7-keV γ ray with the 5814-keV and 5819-keV α-particle energies in (a) is due to the α particles that escape from the DSSD.

FIG. 5. The total projection of the γ-γ matrix of the γ rays in coincidence within 150 ns with the ^{175}Pt α decays detected with the planar detector. The γ rays in coincidence with the 76.7-keV transition in the matrix (b). The γ-γ time-coincidence condition was 90 ns. The whole DSSD was used for the α-particle detection.

and the $E_\alpha = 5819$-keV decay branches. Similarly, the γ rays detected within 150 ns of the detection of the $E_\alpha = 5948$-keV decay branch are shown in Fig. 4(b). The spectra of Fi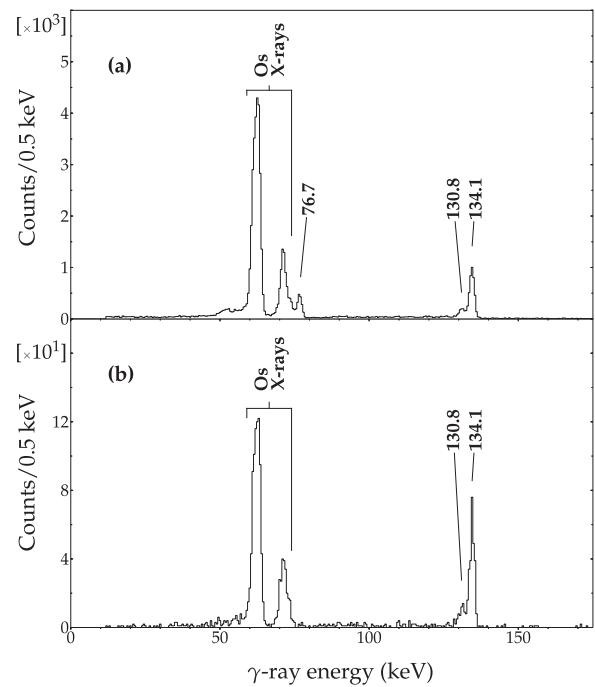gs. 4(a) and 4(b) were also obtained with the focal-plane clover detector, albeit with not as good average energy resolution. The strong 161.6-keV transition shown in Fig. 4(a) is emitted after the α decay of ^{172}Ir to an excited state in ^{168}Re. The α-particle energy and the half-life for the ^{172}Ir α decay from this experiment are 5817(4) keV and 1.81(4) s, respectively. These values are consistent with the values found from Refs. [32,33]. The 91.7-keV transition seen in Fig. 4(b) is correlated within 150 ns with $E_\alpha = 5919(4)$ keV and $t_{\frac{1}{2}} = 1.14(5)$ s, which is consistent with the values reported for the α decay of ^{171}Ir [32,34]. The 76.7-keV, 130.8-keV, 134.1-keV, 207.9-keV, and 211.2-keV ^{171}Os γ rays were observed to be in delayed coincidence with the prompt ^{175}Pt γ rays. The 76.7-keV, 134.1-keV, and 211.2-keV transition energies are the same as reported by Hagberg *et al.* [29], although they mentioned the 76.7-keV transition to be in coincidence only with the favoured α-decay branch. This γ-ray transition was detected in this work in coincidence with the α-decay events corresponding to $E_\alpha = 5814$ keV, 5819 keV, and 5948 keV. The 130.8-keV and 207.9-keV transitions were reported in the in-beam study by Bark *et al.* where the transitions are assumed to be part of the $^5/_2^-$[523] ground-state band of ^{171}Os [35]. The detection of the 130.8-keV and 207.9-keV γ rays, in addition to the known 134.1-keV and 211.2-keV γ rays, following the ^{175}Pt α-decay events implies an identification of a fourth α-decay branch in

^{175}Pt. The α-decay branching ratios for these $E_\alpha = 5814$-keV and 5819-keV α decays were calculated assuming that the branching ratio $b_\alpha = 4.7\%$ given in Ref. [29] is equal to the sum of the two α-decay branches. The total branching ratio was divided according to the total intensities for the 130.8-keV and 134.1-keV transitions. An $M1$ character was assumed for both transitions in this calculation; see Table I.

In a focal plane γ-γ matrix tagged with the ^{175}Pt α decays the 130.8-keV and 134.1-keV transitions are in coincidence with the 76.7-keV transition. The total projection of this matrix is shown in Fig. 5(a), and γ rays in coincidence with the 76.7-keV γ ray are shown in Fig. 5(b). The experimental K-conversion coefficients α_k could not be calculated separately for the 130.8-keV and 134.1-keV transitions using the spectrum in Fig 5(b). However, it was possible to calculate the α_k value for both transitions together. The experimental value obtained is $\alpha_k = I(\text{x} - \text{ray}) \times [I(130.8 \text{ keV}) + I(134.1 \text{ keV})]^{-1} = 2.1(2)$. The measured conversion coefficient was compared with theoretical predictions taken from the BrIcc V2.3 database [36]. The theoretical values for the different α_k sums are 2.04(4), 1.74(3), 0.76(3), and 0.46(1), for $M1 + M1$, $E2(130.8 \text{ keV}) + M1(134.1 \text{ keV})$, $M1(130.8 \text{ keV}) + E2(134.1 \text{ keV})$ and $E2 + E2$ combinations, respectively. The error for the theoretical value comes from the γ-ray error estimate. Based on these results both the 130.8-keV and 134.1-keV transitions were assigned to have an $M1$ character. The α_k for the 76.7-keV transition was also obtained from the focal plane γ-γ matrix, where coincidences with the 130.8-keV and 134.1-keV transitions
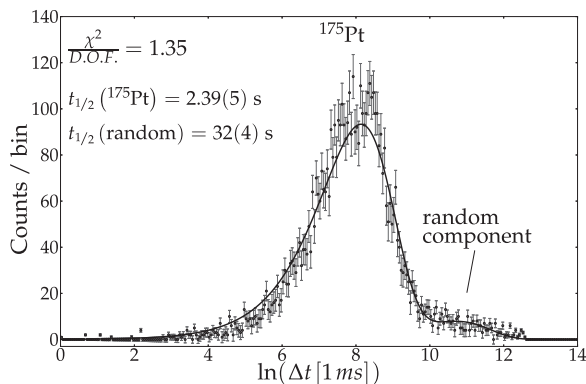
FIG. 6. The two-component fit made to the $\ln(\Delta t)$ time-difference spectrum. The time difference Δt (in 1 ms units) is measured between the recoil and α-decay events. The α-particle energy condition was set for the $E_\alpha = 5948$-keV ^{175}Pt α decays. Additionally, a γ ray detected in the planar detector with the energy of 76.7 keV was demanded within 150 ns after the α-particle detection. Only the low count-rate border area of the DSSD was used for the search of recoil-α correlations.

were demanded separately. The weighted average of the results, $\alpha_k(76.7 \text{ keV}) = 11.6(9)$, is compared with the theoretical value of $\alpha_k(M1) = 9.85(15)$. This suggests that the 76.7-keV transition is also of $M1$ character. It was not possible to determine the multipolarities of the 207.9-keV and 211.2-keV transitions similarly to the 130.8-keV and 134.1-keV transitions.

The fact that all the measured half-lives, where a γ ray is demanded after the detected α decay, are consistent with each other suggests that the 207.9-keV and 211.2-keV transitions belong to ^{171}Os. Also, the 76.7-keV transition plus the 130.8-keV or the 134.1-keV transition sum up to 207.5 keV and 210.8 keV, respectively. The half-life of the ^{175}Pt ground state was measured to be 2.43(4) s, which was calculated as a weighted average of the half-lives given in Table I. The half-lives have been fitted using the method presented by Schmidt *et al.* [37]. In all cases, these data were fitted with a two-component function to take into account the longer half-life of the random component. The recoil-α time difference spectrum with the 5948-keV α-particle energy condition and the result of the two-component fit are shown in Fig. 6.

B. In-beam γ-ray spectroscopy

The observation of excited states of ^{175}Pt was reported for the first time by Cederwall *et al.* [2]. In their work they used a germanium detector array and γ-γ coincidence analysis together with a recoil separator. They reported γ rays from excited states of ^{175}Pt up to level energies of approximately 4.2 MeV. The spins and parities were tentatively assigned based on the systematics. The total prompt γ-ray energy spectrum of ^{175}Pt, from the present data, tagged with the 5948-keV α-particle energy of ^{175}Pt is shown in Fig. 7(a). In this figure the whole DSSD is used when investigating the recoil-α correlations. Several contaminant γ rays can be seen in the energy spectrum, which is due to the high implantation
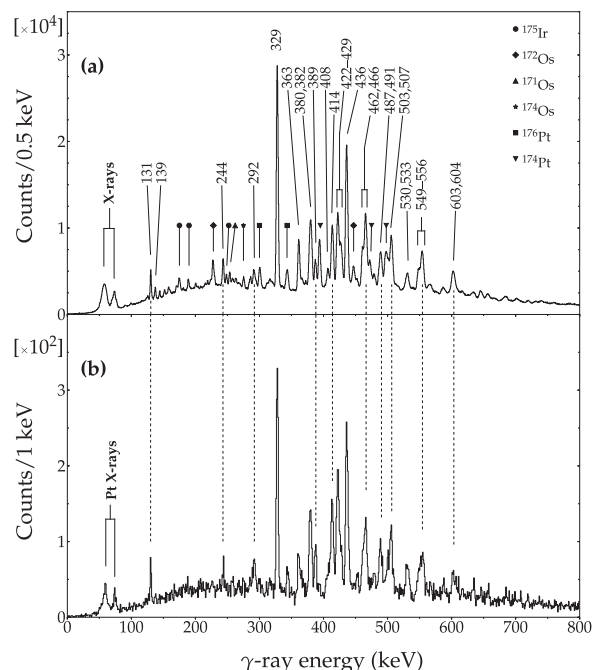

FIG. 7. Total ^{175}Pt α-tagged JUROGAM singles energy spectra in coincidence with an α-decay event in the DSSD. The α-particle energy was demanded to be 5948 keV. The recoil-α correlation time was 7.5 s. In (a) the whole DSSD has been used for the search of recoil-α correlations. The strongest transitions and some of the newly found transitions in ^{175}Pt are highlighted. In (b) only the low-counting horizontal strips of the DSSD were used to correlate the recoil with the α decays. Additionally, a ^{171}Os x ray or a 76.7-keV γ ray, detected by the planar detector following the α-particle detection, was demanded in (b). The contaminant γ rays in (a) originate from the reaction channels, which have relatively large cross sections in the reaction used. The dashed lines between (a) and (b) highlight some of the γ rays belonging to ^{175}Pt.

rate into the DSSD compared with the ^{175}Pt half-life. When using only the low-counting horizontal strips of the DSSD (see Fig. 1), the random coincidences between the recoil- and the α-decay events are reduced. This is demonstrated by Fig. 7(b). The level scheme based on the analysis in this work is shown in Fig. 8. The γ-ray transition energies and the corresponding level energies are listed in Table II. The ordering of the transitions is based on the measured intensities of the transitions and on the coincidence relations between the transitions.

The transitions in the positive-parity band of ^{175}Pt are seen as the most intense peaks in Fig. 7(b). By using recoil-gated triple γ-ray coincidence data, the positive-parity band reported by Cederwall *et al.* [2] was identified. The full DSSD was used for the detection of recoil events. Band 1, based on the $I^\pi = (13/2^+)$ level, was extended to $I^\pi = (49/2^+)$ in the present work. The sum spectrum from double gates to the transitions in band 1 is shown in Fig. 9(a). In Figure 9(b) the sum spectrum of double gates to the transitions in band 2 is shown. The 138.6-keV and 244.1-keV transitions in band 2 are in coincidence with each other and the sum of their energies corresponds to the 382.2-keV transition energy.
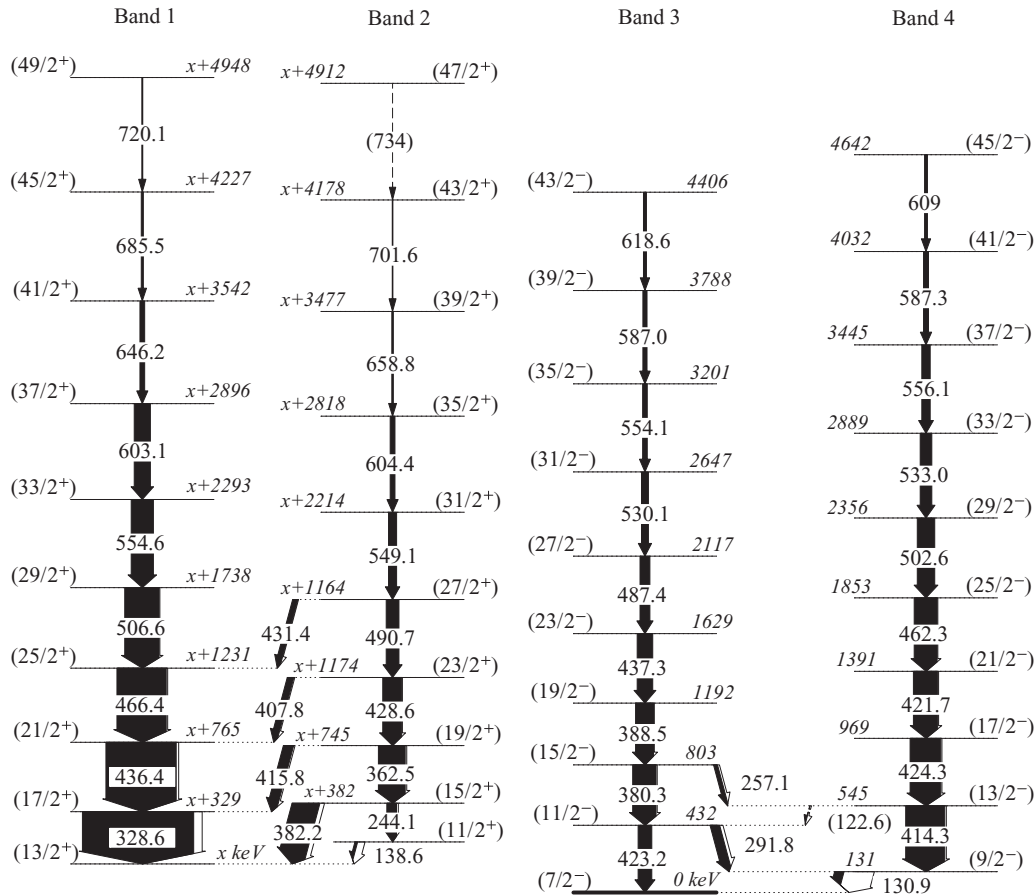
FIG. 8. The proposed level scheme for ^{175}Pt. The spin and parity assignments are based on the measured intensity ratios, angular distributions, the α-decay and ground-state properties of ^{179}Hg, ^{175}Pt, and ^{171}Os and the systematics in this region of nuclei.

The 382.2-keV transition is not in coincidence with either the 138.6-keV or the 244.1-keV transition. Hence the 382.2-keV transition originating from the $I^{\pi} = (15/2^+)$ state is assigned to follow a parallel decay path with the 138.6-keV and 244.1-keV transitions. Two new transitions with energies of 701.6 keV and 734 keV are observed in coincidence with the known transitions in band 2 extending the band up to $I^{\pi} = (47/2^+)$. Figure 9(c) shows γ rays in coincidence with the 436.4-keV and 466.4-keV transitions. The interband 431.4-keV transition originates from the $I^{\pi} = (27/2^+)$ state.

The spectrum of Fig. 7(b) reveals many transitions that are not known to belong to other reaction products. Selecting coincidences with these γ rays shows new transitions in a rotational band in ^{175}Pt. The whole DSSD was used for the α-tagged γ-γ analysis. Due to Compton scattering of the high-energy gamma rays, which also have high intensity, random coincidences are visible in Figs. 10(a)–10(c). The results obtained from the γ-γ analysis were also verified using the triple-coincidence data. Figures 10(a) and 10(b) show γ-ray coincidences with the 130.9-keV and the 421.7-keV transitions, respectively. The 291.8-keV transition is only in coincidence with the 130.9-keV γ ray and not with other transitions in band 4. A second rotational band is observed in coincidence with the 388.5-keV transition, which is shown in Fig. 10(c). These new rotational structures are assumed to

belong to a negative-parity band built on top of the ground state of ^{175}Pt. No linking transitions between the newly observed band structures and the positive-parity band were observed. Based on the systematics of the platinum isotopes we assume the $(13/2^+)$ state to lie at most 200 keV above the $(9/2^-)$ state. The half-life of this state can be estimated using the single-particle Weisskopf estimates for the electromagnetic transition rates [38]. This estimate for the half-life of the $(13/2^+)$ state is of the order of 1 μs. If the excitation energy of the $(13/2^+)$ state compared with the $(9/2^-)$ state is low, the corresponding $M2$ transition would proceed mainly via internal conversion and it would not be detected by the focal-plane germanium detectors. However, if this decay path existed the 130.9-keV $(9/2^-)$ to $(7/2^-)$ transition should have been detected in the focal-plane detectors. Correlation times up to 100 μs between the recoils and γ rays at the focal plane were used, but the 130.9-keV transition was not detected. Another possibility is that the $(13/2^+)$ state lies below the $(9/2^-)$ state in ^{175}Pt. In this case the energy of the $(13/2^+)$ level would be below 130.9 keV. The corresponding half-life estimate for such an $E3$ transition would be of the order of 10 ms. A search for a transition from an isomeric state was carried out up to a 10 ms search time, but revealed no candidates. The nonobservation of the 130.9-keV transition with the focal-plane germanium detectors favors the scenario of an $E3$ transition from a

TABLE II. Table of the γ-ray transition energies, the level energies, the band-head configurations, the spin and parity assignments, and the normalized intensities. The intensities of the transitions are normalized to the $(\frac{17}{2}^+) \to (\frac{13}{2}^+)$ 328.6-keV transition. The band-head configurations are labeled as follows: $\nu_1 = {}^7/2[503]$, $\nu_2 = {}^7/2[514]$, M = mixed $i_{13/2}$.

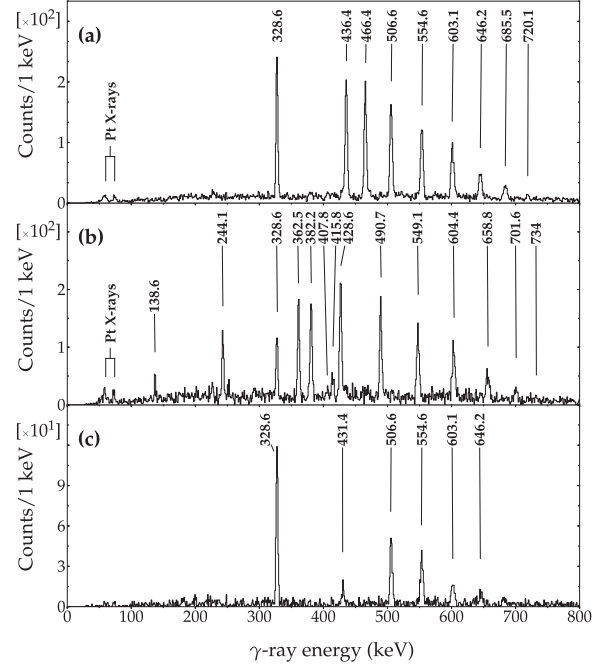| E_γ (keV)	E_{level} (keV)	Band head	J_i^π	J_f^π	I_γ
122.6(7)	546(2)	ν_1/ν_2	$(13/2^-)$	$(11/2^-)$	0.3(2)
130.9(6)	130.9(6)	ν_1/ν_2	$(9/2^-)$	$(7/2^-)$	8.2(5)
138.6(6)	$X+138.6(6)$	M	$(11/2^+)$	$(13/2^+)$	2.4(4)
244.1(4)	$X+382.7(8)$	M	$(15/2^+)$	$(11/2^+)$	8.7(5)
257.1(8)	802(2)	ν_1/ν_2	$(15/2^-)$	$(13/2^-)$	3.5(5)
291.8(6)	422.7(9)	ν_1/ν_2	$(11/2^-)$	$(9/2^-)$	8(1)
328.6(4)	$X+328.6(4)$	M	$(17/2^+)$	$(13/2^+)$	100(2)
362.5(5)	$X+745.2(9)$	M	$(19/2^+)$	$(15/2^-)$	24.1(8)
380.3(4)	803.5(6)	ν_1/ν_2	$(15/2^-)$	$(11/2^-)$	21(2)
382.2(4)	$X+382.2(4)$	M	$(15/2^+)$	$(13/2^+)$	24(4)
388.5(4)	1191.9(7)	ν_1/ν_2	$(19/2^-)$	$(15/2^-)$	16.1(8)
407.8(4)	$X+1173.1(7)$	M	$(23/2^+)$	$(21/2^+)$	5.8(4)
414.3(5)	545.1(8)	ν_1/ν_2	$(13/2^-)$	$(9/2^-)$	35(2)
415.8(4)	$X+744.6(6)$	M	$(19/2^+)$	$(17/2^+)$	9.0(5)
421.7(4)	1391(1)	ν_1/ν_2	$(21/2^-)$	$(17/2^-)$	22(3)
423.2(4)	423.2(4)	ν_1/ν_2	$(11/2^-)$	$(7/2^-)$	12(2)
424.3(4)	969.4(9)	ν_1/ν_2	$(17/2^-)$	$(13/2^-)$	28(3)
428.6(4)	$X+1174(1)$	M	$(23/2^+)$	$(19/2^+)$	17.0(9)
431.4(8)	$X+1663(1)$	M	$(27/2^+)$	$(25/2^+)$	5(2)
436.4(4)	$X+765.3(6)$	M	$(21/2^+)$	$(17/2^+)$	63(2)
437.3(5)	1629.2(9)	ν_1/ν_2	$(23/2^-)$	$(19/2^-)$	14(2)
462.3(5)	1853(1)	ν_1/ν_2	$(25/2^-)$	$(21/2^-)$	21(2)
466.4(4)	$X+1231.7(7)$	M	$(25/2^+)$	$(21/2^+)$	44(2)
487.4(6)	2117(1)	ν_1/ν_2	$(27/2^-)$	$(23/2^-)$	9(2)
490.7(4)	$X+1664(1)$	M	$(27/2^+)$	$(23/2^+)$	11.2(5)
502.6(5)	2356(2)	ν_1/ν_2	$(29/2^-)$	$(25/2^-)$	15(2)
506.6(4)	$X+1738.3(8)$	M	$(29/2^+)$	$(25/2^+)$	30.8(9)
530.1(6)	2647(2)	ν_1/ν_2	$(31/2^-)$	$(27/2^-)$	6(2)
533.0(7)	2889(2)	ν_1/ν_2	$(33/2^-)$	$(29/2^-)$	10(3)
549.1(5)	$X+2214(2)$	M	$(31/2^+)$	$(27/2^+)$	7.1(8)
554.1(7)	3201(2)	ν_1/ν_2	$(35/2^-)$	$(31/2^-)$	4(2)
554.6(4)	$X+2292.9(9)$	M	$(33/2^+)$	$(29/2^+)$	19.6(8)
556.1(7)	3445(2)	ν_1/ν_2	$(37/2^-)$	$(33/2^-)$	7(2)
587.0(7)	3788(2)	ν_1/ν_2	$(39/2^-)$	$(35/2^-)$	3.6(7)
587.3(8)	4032(2)	ν_1/ν_2	$(41/2^-)$	$(37/2^-)$	4.4(9)
603.1(4)	$X+2896(1)$	M	$(37/2^+)$	$(33/2^+)$	14.3(5)
604.4(5)	$X+2818(2)$	M	$(35/2^+)$	$(31/2^+)$	4.2(6)
609(1)	4642(2)	ν_1/ν_2	$(45/2^-)$	$(41/2^-)$	2.5(7)
618.6(8)	4406(2)	ν_1/ν_2	$(43/2^-)$	$(39/2^-)$	2.6(5)
646.2(6)	$X+3542(2)$	M	$(41/2^+)$	$(37/2^+)$	4.2(4)
658.8(5)	$X+3477(2)$	M	$(39/2^+)$	$(35/2^+)$	1.3(3)
685.5(6)	$X+4228(2)$	M	$(45/2^+)$	$(41/2^+)$	1.8(3)
701.6(9)	$X+4178(2)$	M	$(43/2^+)$	$(39/2^+)$	0.6(1)
720.1(7)	$X+4948(2)$	M	$(49/2^+)$	$(45/2^+)$	0.8(2)
734(2)	$X+4912(2)$	M	$(47/2^+)$	$(43/2^+)$	0.4(1)

FIG. 9. The sum spectrum of double gates, set on all transitions from 328.6 keV to 685.5 keV of band 1 (a). The resulting spectrum of summing up the double gates for all transitions from 138.6 keV to 658.8 keV in band 2 (b). Setting a double gate on the 436.4-keV and 466.4-keV transitions (c) highlights the new 431.4-keV interband transition.

A positive value for A_2/A_0 suggests a stretched $\Delta I = 2$ transition, whereas a negative value suggests a stretched $\Delta I = 1$ transition [39]. The results for the A_4/A_0 terms from the fits are inconclusive. For some of the weaker transitions only the ratio of the anisotropy could be measured. It was defined as

$$R = \frac{I_\gamma(157.60°)}{I_\gamma(94.16°) + I_\gamma(85.84°)}, \tag{1}$$

where I_γ is the efficiency corrected γ-ray intensity measured at the given angle. The results for the angular distribution coefficients and the ratios of anisotropy are listed in Table III.

IV. DISCUSSION

Hindrance factors for the ^{175}Pt α-decay branches were calculated using the Rasmussen method [41,42]. When the α decay was known to connect states of different spin, the reduced width calculation was performed assuming $\Delta l = 2$. The calculated results for the reduced widths and the hindrance factors are shown in Table I. According to the calculated hindrance factors, the $E_\alpha = 5948$-keV α-decay branch to the $(7/2^-)$ state is a favoued decay branch as reported in earlier work [29]. The decay to the 211.2-keV level is unhindered if the spin and parity of the final state are assumed to be $(9/2^-)$. However, the $I_f^\pi = (7/2^-)$ possibility cannot be ruled out, in which case the calculated hindrance factor is larger, although the two results agree with each other within the error

state below the $(9/2^-)$ state. Thus the $I^\pi = (13/2^+)$ level is placed in the level scheme with an unspecified excitation energy.

It was possible to fit the angular distribution coefficients A_2/A_0 and A_4/A_0 [39,40] for the strongest transitions in ^{175}Pt.
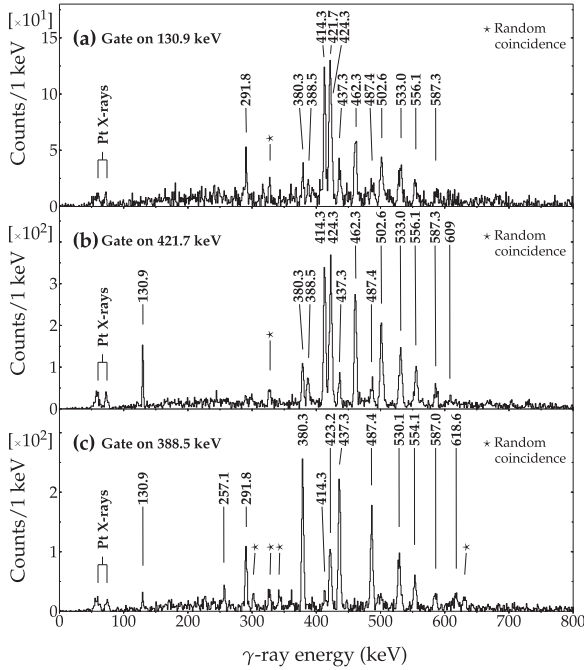
FIG. 10. γ rays belonging to band 4 in coincidence with the 130.9-keV γ rays in the α-tagged γ-γ matrix (a). γ rays in coincidence with the 421.7-keV transition in band 4 (b). Due to energy overlap with the 423.2-keV transition in band 3, some γ rays from band 3 are visible in (b). γ rays in coincidence with the 388.5-keV γ ray in band 3 (c). The recoil-α correlation time was 7.5 s and an α-particle energy condition of 5948-keV was demanded.

limits. The α decays leading to the $(5/2^-)$ ground state and the $(9/2^-)$ 207.9-keV states have hindrance factors 22(4) and 19(6), respectively. This suggests that these states do not belong to

TABLE III. Table of the angular distribution coefficients [40], the intensity ratios and the deduced angular momentum carried away by the photon for the strongest transitions for ^{175}Pt. The anisotropy ratio is calculated as $R = I_\gamma(157.60°) \times [I_\gamma(94.16°) + I_\gamma(85.84°)]^{-1}$.

E_γ (keV)	A_2/A_0	A_4/A_0	R	ΔI ($\hbar$)
130.9(6)[a]	−0.15(8)	0.0(2)	0.82(6)	1
138.6(6)[a]			1.3(2)	2
244.1(4)[a]	0.09(2)	−0.05(4)	1.16(8)	2
291.8(6)[a]	−0.13(8)	0.1(2)	0.92(8)	1
328.6(4)[a]	0.21(1)	−0.05(2)	1.31(5)	2
362.5(5)[a]	0.09(3)	−0.03(5)	1.11(5)	2
382.2(4)[b]			1.0(2)	
388.5(4)[a]	0.11(2)	0.01(2)	1.13(7)	2
423.2(4)[b]			0.9(2)	
428.6(4)[b]			1.1(2)	2
436.4(4)[b]	0.23(4)	−0.03(5)	1.30(8)	2
437.3(5)[b]			1.3(2)	2
466.4(4)[b]	0.29(2)	0.02(3)	1.4(1)	2
487.4(6)[b]			1.0(2)	
506.6(4)[b]			1.3(2)	2
554.6(4)[b]			1.4(2)	2

[a]The data is fitted from the α-tagged singles γ-ray energy spectra.
[b]The data is fitted from the α-tagged γ-γ matrix.

the same configuration as the 76.7-keV $(7/2^-)$ state in ^{171}Os. If the ^{171}Os ground state is based on the $5/2^-[523]$ Nilsson configuration, the $(7/2^-)$ state could have a larger admixture of the $7/2^-[503]$ Nilsson configuration.

The spin and parity of $I^\pi = (7/2^-)$ for the ^{175}Pt ground state can be assigned in two ways. Firstly, the ^{179}Hg ground-state spin and parity have been assigned to be $I^\pi = 7/2^-$ in a focal-plane decay-spectroscopy experiment [43]. Furthermore, the 6.288-MeV α decay from ^{179}Hg most likely populates the ground state of ^{175}Pt [29]. Hagberg *et al.* based their assumption on the α-decay hindrance factor and the fact that they did not see γ rays following the α decay of ^{179}Hg. Secondly, the ground states of $A = 171, 173$ osmium isotopes have been assigned to $I^\pi = (5/2^-)$ [35]. In the present work the 76.7-keV transition in ^{171}Os has been measured to have dipole multipolarity, which implies that the 76.7-keV level has $I = (7/2)$. This is in agreement with the spin assignment of $(7/2)$ by Bark *et al.* [35]. The favored α decay from the ground state of ^{175}Pt populates this 76.7-keV $I^\pi = (7/2^-)$ state in ^{171}Os, therefore the conclusion is that the ^{175}Pt ground state is also $I^\pi = (7/2^-)$. The Nilsson-configuration candidates for the ^{175}Pt ground state are the same as for ^{179}Hg: $7/2^-[514]$ or $7/2^-[503]$, as has been suggested in Ref. [44].

In Fig. 11 the experimental $B(M1)/B(E2)$ ratios are compared with the theoretical values obtained for these two configuration candidates. The experimental $B(M1)/B(E2)$ ratio can be written as [12]

$$\frac{B(M1, I \to I-1)}{B(E2, I \to I-2)}$$
$$= 0.0693 \frac{16\pi}{5} \frac{[E_\gamma(I \to I-2)]^5}{[E_\gamma(I \to I-1)]^3 \lambda(1+\delta^2)}, \quad (2)$$

where the branching ratio $\lambda = I_\gamma(I \to I-2) \times [I_\gamma(I \to I-1)]^{-1}$. The $M1/E2$-mixing ratio δ has been taken to be zero in the calculations. The theoretical $B(M1)/B(E2)$-ratio equation is based on the work of Dönau and Frauendorf [45,46] and the
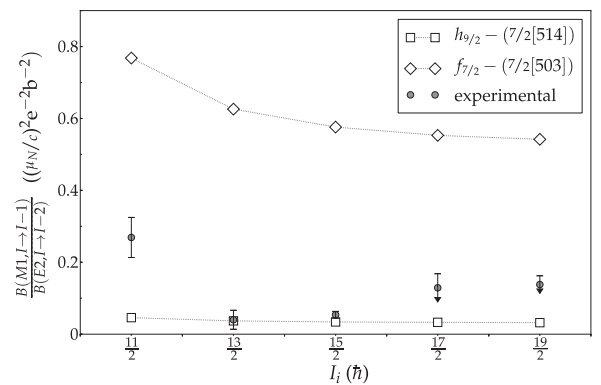

FIG. 11. The experimental $B(M1)/B(E2)$ ratios are plotted and compared with the theoretical values. The theoretical calculations are done for the $h_{9/2}$ (open squares) and $f_{7/2}$ (open diamonds) single-particle orbitals. The two rightmost experimental points are upper-limit estimates for the $B(M1)/B(E2)$ ratio. They have been obtained by estimating the maximum intensity the corresponding $M1$ transition could have, that would not be detected from the γ-ray background.

equation used for the calculations was [12]

$$\frac{B(M1, I \rightarrow I-1)}{B(E2, I \rightarrow I-2)}$$

$$= \frac{12}{5} \frac{K^2}{Q_0^2 \cos^2(30° + \gamma)} \left[1 - \frac{K^2}{(I - 1/2)^2} \right]^{-2}$$

$$\times \left[(g_a - g_R) \left(\sqrt{1 - \frac{K^2}{I^2}} - \frac{i_a}{I} \pm \frac{\Delta e'}{\omega} \right) \right.$$

$$\left. - (g_b - g_R) \frac{i_b}{I} \right]^2. \tag{3}$$

The parameter values used for the calculation are $Q_0 = 6\,e$ b, $\gamma = -21°$, $i_a = 1\,\hbar$, $i_b = 0\,\hbar$, $g_R \approx Z/A = 0.45$. The single-particle g factors for neutrons were calculated to be $g_a(h_{9/2}) = 0.243$ and $g_a(f_{7/2}) = -0.383$ [47], taking $g_s(\text{eff}) = 0.7 \times g_s(\text{free})$. The signature splitting term $\Delta e'$ was taken to be zero in the calculations for the negative-parity states. Figure 11 suggests that the $7/2^-[514]$ configuration from the $h_{9/2}$ orbital is the favored candidate.

The rotational properties of the excited states of ^{175}Pt have been investigated by using the cranked shell-model (CSM) formalism [48,49]. In Figs. 12(a) and 12(b) the relative aligned angular momenta, $i(\omega)$, of the even-Z $N = 97$ isotones from hafnium to platinum have been plotted for the positive- and negative-parity states, respectively. For the aligned angular momentum plots the choice of the reference configuration presents a difficult choice for the analysis of ^{175}Pt. Shape coexistence has been proposed for ^{174}Pt [3,4] and ^{176}Pt [1,2] at low excitation energy, making them unsuitable as reference candidates. The reference parameters for ^{175}Pt, $J_0 = 29\,\text{MeV}^{-1}\hbar^2$, $J_1 = 172\,\text{MeV}^{-3}\hbar^4$, have been taken from the fit of the Harris polynomial [50] to the ^{178}Pt ground state band between the 6^+–14^+ states. With these parameters the relative alignments of the ^{176,178}Pt ground-state bands stay constant above the 8^+ states. These parameters have been used for the alignment plots for all the bands in ^{175}Pt. The experimental results are compared with CSM calculations based on a Woods-Saxon type potential [51,52]. The pairing gaps were calculated at zero rotational frequency and they were allowed to decrease to half of their original values by $\hbar\omega = 0.7$ MeV [53]. The calculated single-particle Routhians for neutrons and protons are shown in Figs. 13(a) and 13(b) and the labeling of the quasiparticle states is given in Table IV. The deformation parameters $\beta_2 = 0.18$, $\beta_4 = 0$, and $\gamma = -21°$ for the calculations were based on the total-Routhian surface (TRS) calculation results in this region [2].

Compared with the Hf, W, and Os isotones the positive- and negative-parity band alignments of ^{175}Pt change sharply at $\hbar\omega \approx 0.2$ MeV. Irregular behavior of the alignment curves at low frequency has been reported earlier, for example in ^{172}Os by Durell et al. [54] who suggest that a change in deformation at low rotational frequency could be responsible for the feature in the observed alignment. In the case of ^{174}Pt [3] and ^{176}Pt [2] the irregularity of the alignment curves is interpreted as a sign of a crossing between the weakly deformed ground-state band and the well deformed intruder band. As for ^{174,176}Pt ground-state configurations [2], the TRS calculations predict
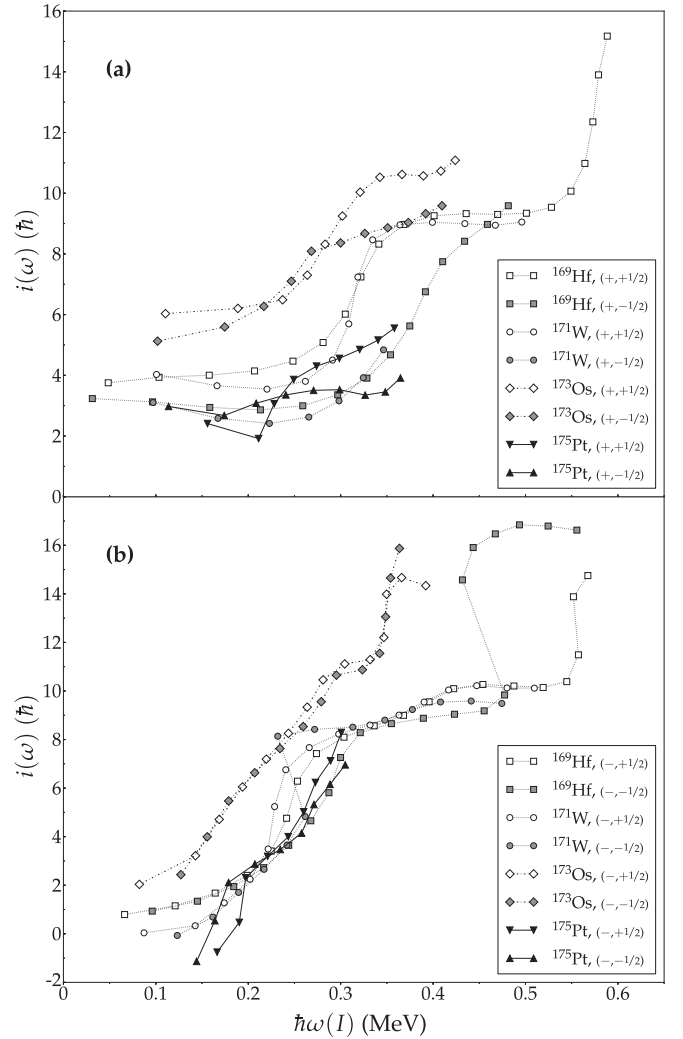

FIG. 12. Relative aligned angular momenta $i(\omega)$ calculated for the negative-parity bands of the $N = 97$ isotones of Hf, W, Os, and Pt (a). The calculated $i(\omega)$ for the positive-parity bands (b) of for the same nuclei as in (a). The reference configuration parameter values for ^{175}Pt were $J_0 = 29\,\text{MeV}^{-1}\hbar^2$, $J_1 = 172\,\text{MeV}^{-3}\hbar^4$. The transition energy, J_0, and J_1 values for ^{171}W and ^{169}Hf were taken from [57,61], respectively. For ^{173}Os the transition energies were taken from [62] and the J_0 and J_1 reference values from [35].

the negative-parity configurations of ^{175}Pt to be γ-soft at low rotational frequencies [7]. The change in deformation of the nucleus would however not be associated with the alignment of quasiparticles, but with an excitation of a proton pair within the rotating core [2,55]. For the positive-parity band of ^{175}Pt this has already been suggested [2] and it is also taken to be the reason for the observed irregularity in the negative-parity band.

The behavior of the alignment of the positive-parity band of ^{175}Pt is quite different from the other isotones of Fig. 12(a). In the case of the positive-parity configuration, the odd neutron occupies the lowest positive-parity state A or B. For this reason the lowest quasineutron AB alignment is blocked. The next available aligned quasineutron configuration is ABC
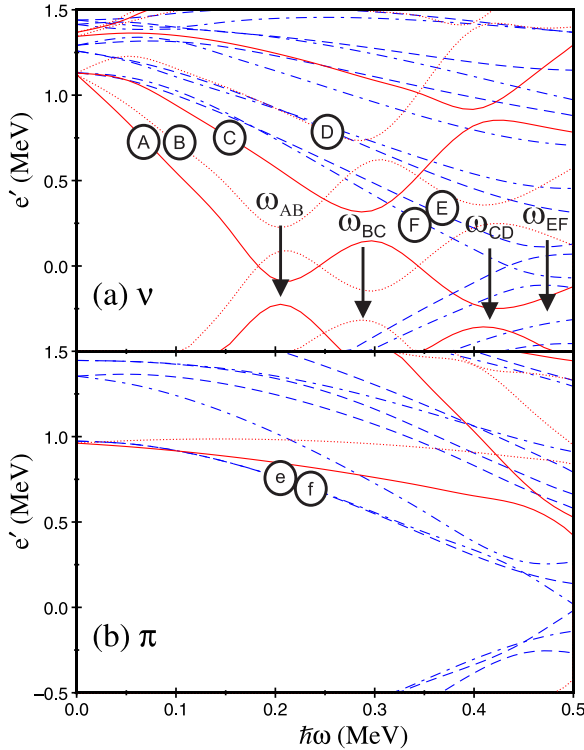
FIG. 13. (Color online) The CSM single-particle Routhians are shown for (a) quasineutrons and (b) quasiprotons as a function of the frequency of the rotation. The four first crossing frequencies are marked with arrows for the quasineutrons on the positive (red color) and negative (blue color) parity orbitals. The quasiparticle labeling is given in Table IV. The deformation parameters used in the calculation were $\beta_2 = 0.18$, $\beta_4 = 0$, and $\gamma = -21°$ [2].

or BAD as has been suggested for ^{169}Hf [56], ^{171}W [57], and ^{173}Os [35]. After the low-frequency alignment change at $\hbar\omega \approx 0.2$ MeV, the alignment of the $(\pi,\alpha) = (+,-\frac{1}{2})$ band stays constant in ^{175}Pt until the very last measured transition. The $(\pi,\alpha) = (+,+\frac{1}{2})$ band shows a gradual alignment increase of $\Delta i \approx 3\hbar$ close to $\hbar\omega = 0.3$ MeV, whereas the Hf, W, and Os isotopes display a better defined alignment gain of $\Delta i \approx 5\hbar$. The calculations predict the second crossing in ^{175}Pt to be due to the alignment of the BC and AD quasineutrons similarly to the lighter isotones. This crossing frequency from the calculations is $\hbar\omega \approx 0.28$ MeV and the estimated alignment

gain from Fig. 13(a) is 6 $\hbar$. The experimentally observed gradual alignment of the $(+,+\frac{1}{2})$ band is in agreement with the theoretical result. The observed gradual alignment can be explained as a sign of a strong interaction between the crossing bands [58] as has been suggested for ^{173}Os [59]. Only half of the predicted alignment gain is seen, possibly due to bands 1 and 2 not being observed to high enough angular momenta. The unobserved crossing in the $(+,-\frac{1}{2})$ band is in disagreement with the calculated results. In Ref. [2] the unfavored $(\alpha = -\frac{1}{2})$ signature has been shown to have little γ-deformation polarizing capacity compared with the favored $(\alpha = +\frac{1}{2})$ signature. The CSM calculations are performed using fixed deformation parameters, thus not allowing one to take the change in deformation between the signature partners into account. It is also worth pointing out that the initial alignments of the positive-parity bands of ^{175}Pt in Fig. 12 are low compared to the calculated results for A and B configurations. Thus the observation of a clear A (B) → ABC (BAD) alignment is not evident.

The negative-parity band alignment of ^{175}Pt resembles that of the lighter $N = 97$ isotones. The alignment plots for bands 3 and 4 are show in Fig. 12(b). When the odd neutron is occupying a negative-parity state, the AB alignment is not blocked, making it a likely candidate for the observed alignments [35,56,57]. The AB alignment is also assumed to take place in the negative-parity band of ^{175}Pt starting at $\hbar\omega = 0.2$ MeV. This agrees with the calculated results of Fig. 13(a). As for the positive-parity bands of the $N = 97$ isotones, the lack of back bending is assumed to be caused by the strong interaction between the crossing quasiparticle bands. The alignment gain for the ^{175}Pt band, after the low-frequency kink, is $\Delta i \approx 6$ $\hbar$. Estimating the theoretical value from Fig. 13(a) gives $\Delta i_{AB} = 10$ $\hbar$. However, the alignment curves for ^{175}Pt do not level off, making it difficult to estimate the total gained alignment. The possibility of a proton alignment in the frequency range of $\hbar\omega = (0.2–0.3)$ MeV was shown to be unlikely in this mass region [59,60], whereas the alignments seen at $\hbar\omega \approx 0.5$ MeV in the positive- and negative-parity band of ^{169}Hf are assumed to be due to proton alignment [61]. As shown in Fig. 13(b), the calculations made in this work show also that the quasiprotons are unlikely to align before $\hbar\omega = 0.4$ MeV.

V. CONCLUSIONS

A new α-decay branch in ^{175}Pt has been established leading to the known 207.9-keV $I^\pi = (9/2^-)$ state in ^{171}Os. A negative-parity band has been identified in ^{175}Pt and the known positive-parity band has been extended up to $I^\pi = (49/2^+)$. The negative-parity band is assigned to be based on the $(7/2^-)$ ground state of ^{175}Pt. Both the positive- and negative-parity bands show changes in the relative aligned angular momentum plots around $\hbar\omega \approx 0.2$ MeV. It is argued that these changes are due to the unaligned proton-pair excitation within the rotating core of ^{175}Pt, leading to a change in the deformation of the core. The negative-parity band alignments are interpreted to be similar to the lighter $N = 97$ isotones, suggesting gradual AB-neutron alignment due to strong band

TABLE IV. The quasi-particle labeling used in this work.

Label	Parity, signature (π,α)	Main shell-model component
A	$\nu(+,+)_1$	$i_{13/2}$
B	$\nu(+,-)_1$	$i_{13/2}$
C	$\nu(+,+)_2$	$i_{13/2}$
D	$\nu(+,-)_2$	$i_{13/2}$
E	$\nu(-,+)_1$	$h_{9/2}/f_{7/2}$
F	$\nu(-,-)_1$	$h_{9/2}/f_{7/2}$
e	$\pi(-,+)_1$	$h_{9/2}/h_{11/2}$
f	$\pi(-,-)_1$	$h_{9/2}/h_{11/2}$

interaction between the crossing bands. This is supported by the CSM calculation results. The positive-parity band of ^{175}Pt shows markedly different alignment behavior compared with the lighter $N = 97$ isotones. Support for the A→ABC crossing is given by the CSM calculations, but the predicted B→BAD crossing is not observed. The low-spin alignment behavior of the excited states in ^{175}Pt, together with the CSM results are, at least qualitatively, in agreement with the picture of coexisting shapes in the neighboring $A = 174,176$ Pt isotopes [2–4].

[1] G. D. Dracoulis, A. E. Stuchbery, A. P. Byrne, A. R. Poletti, S. J. Poletti, J. Gerl, and R. A. Bark, J. Phys. G **12**, L97 (1986).

[2] B. Cederwall, R. Wyss, A. Johnson, J. Nyberg, B. Fant, R. Chapman, D. Clarke, F. Khazaie, J. C. Lisle, J. N. Mo, J. Simpson, and I. Thorslund, Z. Phys. A At. Nuclei **337**, 283 (1990).

[3] G. D. Dracoulis, B. Fabricius, A. E. Stuchbery, A. O. Macchiavelli, W. Korten, F. Azaiez, E. Rubel, M. A. Deleplanque, R. M. Diamond, and F. S. Stephens, Phys. Rev. C **44**, R1246 (1991).

[4] J. TM. Goon, D. J. Hartley, L. L. Riedinger, M. P. Carpenter, F. G. Kondev, R. V. F. Janssens, K. H. Abu Saleem, I. Ahmad, H. Amro, J. A. Cizewski, C. N. Davids, M. Danchev, T. L. Khoo, A. Heinz, T. Lauritsen, W. C. Ma, G. L. Poli, J. Ressler, W. Reviol, D. Seweryniak, M. B. Smith, I. Wiedenhöver, and J.-y. Zhang, Phys. Rev. C **70**, 014309 (2004).

[5] R. Bengtsson, J.-y. Zhang, J. H. Hamilton, and L. K. Peker, J. Phys. G **12**, L223 (1986).

[6] R. Bengtsson, T. Bengtsson, J. Dudek, G. Leander, W. Nazarewicz, and J.-y. Zhang, Phys. Lett. B **183**, 1 (1987).

[7] Th. Hilberath, St. Becker, G. Bollen, H.-J. Kluge, U. Krönert, G. Passler, J. Rikovska, and R. Wyss, Z. Phys. A Hadrons Nuclei **342**, 1 (1992).

[8] P. M. Davidson, G. D. Dracoulis, T. Kibédi, A. P. Byrne, S. S. Anderssen, A. M. Baxter, B. Fabricius, G. J. Lane, and A. E. Stuchbery, Nucl. Phys. A **657**, 219 (1999).

[9] B. Cederwall, T. Bäck, R. Bark, S. Törmänen, S. Ødegård, S. King, J. Simpson, R. D. Page, N. Amzal, D. M. Cullen, P. T. Greenlees, A. Keenan, R. Lemmon, J. Cocks, K. Helariutta, P. Jones, R. Julin, S. Juutinen, H. Kettunen, H. Kankaanpää, P. Kuusiniemi, M. Leino, M. Muikku, P. Rahkila, A. Savelius, J. Uusitalo, P. Magierski, and R. Wyss, Phys. Lett. B **443**, 69 (1998).

[10] D. T. Joss, J. Simpson, D. E. Appelbe, C. J. Barton, D. D. Warner, K. Lagergren, B. Cederwall, B. Hadinia, S. Eeckhaudt, T. Grahn, P. T. Greenlees, P. M. Jones, R. Julin, S. Juutinen, H. Kettunen, M. Leino, A.-P. Leppänen, P. Nieminen, J. Pakarinen, J. Perkowski, P. Rahkila, C. Scholey, J. Uusitalo, K. Van de Vel, R. D. Page, E. S. Paul, D. R. Wiseman, and M. A. Riley, Phys. Rev. C **74**, 014302 (2006).

[11] M. B. Gómez Hornillos, D. O'Donnell, J. Simpson, D. T. Joss, L. Bianco, B. Cederwall, T. Grahn, P. T. Greenlees, B. Hadinia, P. Jones, R. Julin, S. Juutinen, S. Ketelhut, M. Labiche, M. Leino, M. Nyman, R. D. Page, E. S. Paul, M. Petri, P. Peura, P. Rahkila, P. Ruotsalainen, M. Sandzelius, P. J. Sapple, J. Sarén, C. Scholey, J. Sorri, J. Thomson, and J. Uusitalo, Phys. Rev. C **79**, 064314 (2009).

[12] G. D. Dracoulis, B. Fabricius, R. A. Bark, A. E. Stuchbery, D. G. Popescu, and T. Kibédi, Nucl. Phys. A **510**, 533 (1990).

[13] C. W. Beausang, S. A. Forbes, P. Fallon, P. J. Nolan, P. J. Twin, J. N. Mo, J. C. Lisle, M. A. Bentley, J. Simpson, F. A. Beck, D. Curien, G. deFrance, G. Duchêne, and D. Popescu, Nucl. Instrum. Methods Phys. Res. Sec. A **313**, 37 (1992).

[14] C. Rossi Alvarez, Nucl. Phys. News **3**, 10 (1993).

[15] M. Leino, J. Äystö, T. Enqvist, P. Heikkinen, A. Jokinen, M. Nurmia, A. Ostrowski, W. H. Trzaska, J. Uusitalo, K. Eskola, P. Armbruster, and V. Ninov, Nucl. Instrum. Methods Phys. Res. Sec. B **99**, 653 (1995).

[16] R. D. Page, A. N. Andreyev, D. E. Appelbe, P. A. Butler, S. J. Freeman, P. T. Greenlees, R. D. Herzberg, D. G. Jenkins, G. D. Jones, P. Jones, D. T. Joss, R. Julin, H. Kettunen, M. Leino, P. Rahkila, P. H. Regan, J. Simpson, J. Uusitalo, S. M. Vincent, and R. Wadsworth, Nucl. Instrum. Methods Phys. Res. Sec. B **204**, 634 (2003).

[17] R. D. Page, P. J. Woods, R. A. Cunningham, T. Davinson, N. J. Davis, A. N. James, K. Livingston, P. J. Sellin, and A. C. Shotter, Phys. Rev. C **53**, 660 (1996).

[18] I. H. Lazarus, D. E. Appelbe, P. A. Butler, P. J. Coleman-Smith, J. R. Cresswell, S. J. Freeman, R. D. Herzberg, I. Hibbert, D. T. Joss, S. C. Letts, R. D. Page, V. F. E. Pucknell, P. H. Regan, J. Sampson, J. Simpson, J. Thornhill, and R. Wadsworth, IEEE Trans. Nucl. Sci. **48**, 567 (2001).

[19] P. Rahkila, Nucl. Instrum. Methods Phys. Res. Sec. A **595**, 637 (2008).

[20] D. C. Radford, Nucl. Instrum. Methods Phys. Res. Sec. A **361**, 306 (1995).

[21] D. C. Radford, Nucl. Instrum. Methods Phys. Res. Sec. A **361**, 297 (1995).

[22] K.-H. Schmidt, R. S. Simon, J.-G. Keller, F. P. Heßberger, G. Münzenberg, B. Quint, H.-G. Clerc, W. Schwab, U. Gollerthan, and C.-C. Sahm, Phys. Lett. B **168**, 39 (1986).

[23] R. S. Simon, K.-H. Schmidt, F. P. Heßberger, S. Hlavac, M. Honusek, G. Münzenberg, H.-G. Clerc, U. Gollerthan, and W. Schwab, Z. Phys. A At. Nuclei **325**, 197 (1986).

[24] M. S. Basunia, Nucl. Data Sheets **102**, 719 (2004).

[25] D. O'Donnell, J. Simpson, C. Scholey, T. Back, P. T. Greenlees, U. Jakobsson, P. Jones, D. T. Joss, D. S. Judson, R. Julin, S. Juutinen, S. Ketelhut, M. Labiche, M. Leino, M. Nyman, R. D. Page, P. Peura, P. Rahkila, P. Ruotsalainen, M. Sandzelius, P. J. Sapple, J. Saren, J. Thomson, J. Uusitalo, and H. V. Watkins, Phys. Rev. C **79**, 051304 (2009).

[26] D. T. Joss, S. L. King, R. D. Page, J. Simpson, A. Keenan, N. Amzal, T. Bäck, M. A. Bentley, B. Cederwall, J. F. C.

Cocks, D. M. Cullen, P. T. Greenlees, K. Helariutta, P. M. Jones, R. Julin, S. Juutinen, H. Kankaanpää, H. Kettunen, P. Kuusiniemi, M. Leino, M. Muikku, A. Savelius, J. Uusitalo, and S. J. Williams, Nucl. Phys. A **689**, 631 (2001).

[27] A. Siivola, Nucl. Phys. **84**, 385 (1966).

[28] H. Gauvin, R. L. Hahn, Y. Le Beyec, M. Lefort, and J. Livet, Nucl. Phys. A **208**, 360 (1973).

[29] E. Hagberg, P. G. Hansen, P. Hornshøj, B. Jonson, S. Mattsson, and P. Tidemand-Petersson, Nucl. Phys. A **318**, 29 (1979).

[30] J. G. Keller, K.-H. Schmidt, F. P. Heßberger, G. Münzenberg, W. Reisdorf, H.-G. Clerc, and C.-C. Sahm, Nucl. Phys. A **452**, 173 (1986).

[31] C. M. Baglin, Nucl. Data Sheets **96**, 611 (2002).

[32] W.-D. Schmidt-Ott, H. Salewski, F. Meissner, U. Bosch-Wicke, P. Koschel, V. Kunze, and R. Michaelsen, Nucl. Phys. A **545**, 646 (1992).

[33] C. M. Baglin, Nucl. Data Sheets **111**, 1807 (2010).

[34] C. M. Baglin, Nucl. Data Sheets **90**, 431 (2000).

[35] R. A. Bark, G. D. Dracoulis, and A. E. Stuchbery, Nucl. Phys. A **514**, 503 (1990).

[36] T. Kibédi, T. W. Burrows, M. B. Trzhaskovskaya, P. M. Davidson, and C. W. Nestor, Jr., Nucl. Instrum. Methods Phys. Res. Sec. A **589**, 202 (2008).

[37] K.-H. Schmidt, C.-C. Sahm, K. Pielenz, and H.-G. Clerc, Z. Phys. A At. Nuclei **316**, 19 (1984).

[38] V. F. Weisskopf, Phys. Rev. **83**, 1073 (1951).

[39] R. M. Diamond, E. Matthias, J. O. Newton, and F. S. Stephens, Phys. Rev. Lett. **16**, 1205 (1966).

[40] J. O. Newton, F. S. Stephens, R. M. Diamond, K. Kotajima, and E. Matthias, Nucl. Phys. A **95**, 357 (1967).

[41] J. O. Rasmussen, Phys. Rev. **113**, 1593 (1959).

[42] J. O. Rasmussen, Phys. Rev. **115**, 1675 (1959).

[43] D. G. Jenkins, A. N. Andreyev, R. D. Page, M. P. Carpenter, R. V. F. Janssens, C. J. Lister, F. G. Kondev, T. Enqvist, P. T. Greenlees, P. M. Jones, R. Julin, S. Juutinen, H. Kettunen, P. Kuusiniemi, M. Leino, A.-P. Leppännen, P. Nieminen, J. Pakarinen, P. Rahkila, J. Uusitalo, C. D. O'Leary, P. Raddon, A. Simons, R. Wadsworth, and D. T. Joss, Phys. Rev. C **66**, 011301 (2002).

[44] F. G. Kondev, M. P. Carpenter, R. V. F. Janssens, C. J. Lister, K. Abu Saleem, I. Ahmad, H. Amro, J. Caggiano, C. N. Davids, A. Heinz, B. Herskind, T. L. Khoo, T. Lauritsen, W. C. Ma, J. J. Ressler, W. Reviol, L. L. Riedinger, D. G. Sarantites, D. Seweryniak, S. Siem, A. A. Sonzogni, P. G. Varmette, and I. Wiedenhöver, Phys. Lett. B **528**, 221 (2002).

[45] F. Dönau and S. Frauendorf, in *High Angular Momentum Properties of Nuclei*, edited by N. Johnson (Hardwood Academic, New York, 1983), pp. 143–160.

[46] F. Dönau, Nucl. Phys. A **471**, 469 (1987).

[47] J. M. Blatt and V. F. Weisskopf, *Theoretical Nuclear Physicss*, 5th ed. (John Wiley & Sons, New York, 1960), p. 39.

[48] R. Bengtsson and S. Frauendorf, Nucl. Phys. A **327**, 139 (1979).

[49] R. Bengtsson, S. Frauendorf, and F.-R. May, At. Data Nucl. Data Tables **35**, 15 (1986).

[50] S. M. Harris, Phys. Rev. **138**, B509 (1965).

[51] W. Nazarewicz, J. Dudek, R. Bengtsson, T. Bengtsson, and I. Ragnarsson, Nucl. Phys. A **435**, 397 (1985).

[52] S. Cwiok, J. Dudek, W. Nazarewicz, J. Skalski, and T. Werner, Comput. Phys. Commun. **46**, 379 (1987).

[53] R. Wyss, J. Nyberg, A. Johnson, R. Bengtsson, and W. Nazarewicz, Phys. Lett. B **215**, 211 (1988).

[54] J. L. Durell, G. D. Dracoulis, C. Fahlander, and A. P. Byrne, Phys. Lett. B **115**, 367 (1982).

[55] R. A. Bark, J. Phys. G: Nucl. Part. Phys. **17**, 1209 (1991).

[56] W. B. Gao, I. Y. Lee, C. Baktash, R. Wyss, J. H. Hamilton, C. M. Steele, C. H. Yu, N. R. Johnson, and F. K. McGowan, Phys. Rev. C **44**, 1380 (1991).

[57] J. Espino, J. D. Garrett, G. B. Hagemann, P. O. Tjøm, C.-H. Yu, M. Bergström, L. Carlén, L. P. Ekström, J. Lyttkens-Lindén, H. Ryde, R. Bengtsson, T. Bengston, R. Chapman, D. Clarke, F. Khazaie, J. C. Lisle, and J. N. Mo, Nucl. Phys. A **567**, 377 (1994).

[58] F. S. Stephens and R. S. Simon, Nucl. Phys. A **183**, 257 (1972).

[59] J. C. Wells, N. R. Johnson, C. Baktash, I. Y. Lee, F. K. McGowan, M. A. Riley, A. Virtanen, and J. Dudek, Phys. Rev. C **40**, 725 (1989).

[60] F. K. McGowan, N. R. Johnson, I. Y. Lee, C. Baktash, J. W. McConnell, M. N. Rao, M. Oshima, J. C. Wells, A. Larabee, L. L. Riedinger, R. Bengtsson, and Z. Xing, Nucl. Phys. A **530**, 490 (1991).

[61] K. A. Schmidt, M. Bergström, G. B. Hagemann, B. Herskind, G. Sletten, P. G. Varmette, J. Domscheit, H. Hübel, S. W. Ødegård, S. Frattini, A. Bracco, B. Million, M. P. Carpenter, R. V. F. Janssens, T. L. Khoo, T. Lauritsen, C. J. Lister, S. Siem, I. Wiedenhöver, D. J. Hartley, L. L. Riedinger, A. Maj, W. C. Ma, and R. Terry, Eur. Phys. J. A **12**, 15 (2001).

[62] C. A. Kalfas, S. Kossionides, C. T. Papadopoulos, R. Vlastou, L. Hildingsson, W. K. Lamra, Th. Lindblad, C. G. Lindén, R. Wyss, J. Gizon, S. Juutinen, R. Chapman, D. Clarke, F. Khazaie, J. C. Lisle, and J. N. Mo, Nucl. Phys. A **526**, 205 (1991).